EUROPEAN ORGANIZATION FOR NUCLEAR RESEARCH

CERN-EP/98-16
February 3, 1998

Measurements of the Structure of Quark and Gluon Jets in Hadronic Z Decays

The ALEPH Collaboration

Abstract

An experimental investigation of the structure of identified quark and gluon jets is presented. Observables related to both the global and internal structure of jets are measured; this allows for tests of QCD over a wide range of transverse momentum scales. The observables include distributions of jet-shape variables, the mean and standard deviation of the subjet multiplicity distribution and the fragmentation function for charged particles. The data are compared with predictions of perturbative QCD as well as QCD-based Monte Carlo models. In certain kinematic regions the measurements are sensitive mainly to perturbatively calculable effects, allowing for a test of QCD. The comparisons are also extended into regions where nonperturbative effects become large, and in this way the transition from hard to soft QCD is investigated. It is found that by including leading and next-to-leading logarithmic contributions in the QCD predictions, the agreement with the data can be extended to lower transverse momentum scales, especially for gluon jets.

Submitted to European Physical Journal C

The ALEPH Collaboration

R. Barate, D. Buskulic, D. Decamp, P. Ghez, C. Goy, J.-P. Lees, A. Lucotte, E. Merle, M.-N. Minard, J.-Y. Nief, B. Pietrzyk

Laboratoire de Physique des Particules (LAPP), IN^{2}P^3-CNRS, 74019 Annecy-le-Vieux Cedex, France

R. Alemany, G. Boix, M.P. Casado, M. Chmeissani, J.M. Crespo, M. Delfino, E. Fernandez, M. Fernandez-Bosman, Ll. Garrido,[15] E. Graugès, A. Juste, M. Martinez, G. Merino, R. Miquel, Ll.M. Mir, I.C. Park, A. Pascual, J.A. Perlas, I. Riu, F. Sanchez

Institut de Física d'Altes Energies, Universitat Autònoma de Barcelona, 08193 Bellaterra (Barcelona), Spain[7]

A. Colaleo, D. Creanza, M. de Palma, G. Gelao, G. Iaselli, G. Maggi, M. Maggi, S. Nuzzo, A. Ranieri, G. Raso, F. Ruggieri, G. Selvaggi, L. Silvestris, P. Tempesta, A. Tricomi,[3] G. Zito

Dipartimento di Fisica, INFN Sezione di Bari, 70126 Bari, Italy

X. Huang, J. Lin, Q. Ouyang, T. Wang, Y. Xie, R. Xu, S. Xue, J. Zhang, L. Zhang, W. Zhao

Institute of High-Energy Physics, Academia Sinica, Beijing, The People's Republic of China[8]

D. Abbaneo, U. Becker, P. Bright-Thomas, D. Casper, M. Cattaneo, V. Ciulli, G. Dissertori, H. Drevermann, R.W. Forty, M. Frank, R. Hagelberg, J.B. Hansen, J. Harvey, P. Janot, B. Jost, I. Lehraus, P. Mato, A. Minten, L. Moneta,[21] A. Pacheco, J.-F. Pusztaszeri,[23] F. Ranjard, L. Rolandi, D. Rousseau, D. Schlatter, M. Schmitt,[25] O. Schneider, W. Tejessy, F. Teubert, I.R. Tomalin, H. Wachsmuth, A. Wagner[20]

European Laboratory for Particle Physics (CERN), 1211 Geneva 23, Switzerland

Z. Ajaltouni, F. Badaud, G. Chazelle, O. Deschamps, A. Falvard, C. Ferdi, P. Gay, C. Guicheney, P. Henrard, J. Jousset, B. Michel, S. Monteil, J-C. Montret, D. Pallin, P. Perret, F. Podlyski, J. Proriol, P. Rosnet

Laboratoire de Physique Corpusculaire, Université Blaise Pascal, IN^{2}P^3-CNRS, Clermont-Ferrand, 63177 Aubière, France

J.D. Hansen, J.R. Hansen, P.H. Hansen, B.S. Nilsson, B. Rensch, A. Wäänänen

Niels Bohr Institute, 2100 Copenhagen, Denmark[9]

G. Daskalakis, A. Kyriakis, C. Markou, E. Simopoulou, I. Siotis, A. Vayaki

Nuclear Research Center Demokritos (NRCD), Athens, Greece

A. Blondel, G. Bonneaud, J.-C. Brient, P. Bourdon, A. Rougé, M. Rumpf, A. Valassi,[6] M. Verderi, H. Videau

Laboratoire de Physique Nucléaire et des Hautes Energies, Ecole Polytechnique, IN^{2}P^3-CNRS, 91128 Palaiseau Cedex, France

E. Focardi, G. Parrini, K. Zachariadou

Dipartimento di Fisica, Università di Firenze, INFN Sezione di Firenze, 50125 Firenze, Italy

M. Corden, C. Georgiopoulos, D.E. Jaffe

Supercomputer Computations Research Institute, Florida State University, Tallahassee, FL 32306-4052, USA [13,14]

A. Antonelli, G. Bencivenni, G. Bologna,[4] F. Bossi, P. Campana, G. Capon, F. Cerutti, V. Chiarella, G. Felici, P. Laurelli, G. Mannocchi,[5] F. Murtas, G.P. Murtas, L. Passalacqua, M. Pepe-Altarelli

Laboratori Nazionali dell'INFN (LNF-INFN), 00044 Frascati, Italy

L. Curtis, A.W. Halley, J.G. Lynch, P. Negus, V. O'Shea, C. Raine, J.M. Scarr, K. Smith, P. Teixeira-Dias, A.S. Thompson, E. Thomson

Department of Physics and Astronomy, University of Glasgow, Glasgow G12 8QQ,United Kingdom[10]

O. Buchmüller, S. Dhamotharan, C. Geweniger, G. Graefe, P. Hanke, G. Hansper, V. Hepp, E.E. Kluge, A. Putzer, J. Sommer, K. Tittel, S. Werner, M. Wunsch

Institut für Hochenergiephysik, Universität Heidelberg, 69120 Heidelberg, Fed. Rep. of Germany[16]

R. Beuselinck, D.M. Binnie, W. Cameron, P.J. Dornan,[2] M. Girone, S. Goodsir, E.B. Martin, N. Marinelli, A. Moutoussi, J. Nash, J.K. Sedgbeer, P. Spagnolo, M.D. Williams

Department of Physics, Imperial College, London SW7 2BZ, United Kingdom[10]

V.M. Ghete, P. Girtler, E. Kneringer, D. Kuhn, G. Rudolph

Institut für Experimentalphysik, Universität Innsbruck, 6020 Innsbruck, Austria[18]

A.P. Betteridge, C.K. Bowdery, P.G. Buck, P. Colrain, G. Crawford, A.J. Finch, F. Foster, G. Hughes, R.W.L. Jones, M.I. Williams

Department of Physics, University of Lancaster, Lancaster LA1 4YB, United Kingdom[10]

I. Giehl, A.M. Greene, C. Hoffmann, K. Jakobs, K. Kleinknecht, G. Quast, B. Renk, E. Rohne, H.-G. Sander, P. van Gemmeren, C. Zeitnitz

Institut für Physik, Universität Mainz, 55099 Mainz, Fed. Rep. of Germany[16]

J.J. Aubert, C. Benchouk, A. Bonissent, G. Bujosa, J. Carr,[2] P. Coyle, F. Etienne, O. Leroy, F. Motsch, P. Payre, M. Talby, A. Sadouki, M. Thulasidas, K. Trabelsi

Centre de Physique des Particules, Faculté des Sciences de Luminy, IN^{2}P^3-CNRS, 13288 Marseille, France

M. Aleppo, M. Antonelli, F. Ragusa

Dipartimento di Fisica, Università di Milano e INFN Sezione di Milano, 20133 Milano, Italy

R. Berlich, W. Blum, V. Büscher, H. Dietl, G. Ganis, H. Kroha, G. Lütjens, C. Mannert, W. Männer, H.-G. Moser, S. Schael, R. Settles, H. Seywerd, H. Stenzel, W. Wiedenmann, G. Wolf

Max-Planck-Institut für Physik, Werner-Heisenberg-Institut, 80805 München, Fed. Rep. of Germany[16]

J. Boucrot, O. Callot, S. Chen, A. Cordier, M. Davier, L. Duflot, J.-F. Grivaz, Ph. Heusse, A. Höcker, A. Jacholkowska, D.W. Kim,[12] F. Le Diberder, J. Lefrançois, A.-M. Lutz, M.-H. Schune, E. Tournefier, J.-J. Veillet, I. Videau, D. Zerwas

Laboratoire de l'Accélérateur Linéaire, Université de Paris-Sud, IN^{2}P^3-CNRS, 91405 Orsay Cedex, France

P. Azzurri, G. Bagliesi,[2] G. Batignani, S. Bettarini, T. Boccali, C. Bozzi, G. Calderini, M. Carpinelli, M.A. Ciocci, R. Dell'Orso, R. Fantechi, I. Ferrante, L. Foà,[1] F. Forti, A. Giassi, M.A. Giorgi, A. Gregorio, F. Ligabue, A. Lusiani, P.S. Marrocchesi, A. Messineo, F. Palla, G. Rizzo, G. Sanguinetti, A. Sciabà, R. Tenchini, G. Tonelli,[19] C. Vannini, A. Venturi, P.G. Verdini

Dipartimento di Fisica dell'Università, INFN Sezione di Pisa, e Scuola Normale Superiore, 56010 Pisa, Italy

G.A. Blair, L.M. Bryant, J.T. Chambers, M.G. Green, T. Medcalf, P. Perrodo, J.A. Strong, J.H. von Wimmersperg-Toeller

Department of Physics, Royal Holloway & Bedford New College, University of London, Surrey TW20 OEX, United Kingdom[10]

D.R. Botterill, R.W. Clifft, T.R. Edgecock, S. Haywood, P.R. Norton, J.C. Thompson, A.E. Wright

Particle Physics Dept., Rutherford Appleton Laboratory, Chilton, Didcot, Oxon OX11 OQX, United Kingdom[10]

B. Bloch-Devaux, P. Colas, S. Emery, W. Kozanecki, E. Lançon,[2] M.-C. Lemaire, E. Locci, P. Perez, J. Rander, J.-F. Renardy, A. Roussarie, J.-P. Schuller, J. Schwindling, A. Trabelsi, B. Vallage

CEA, DAPNIA/Service de Physique des Particules, CE-Saclay, 91191 Gif-sur-Yvette Cedex, France[17]

S.N. Black, J.H. Dann, R.P. Johnson, H.Y. Kim, N. Konstantinidis, A.M. Litke, M.A. McNeil, G. Taylor

Institute for Particle Physics, University of California at Santa Cruz, Santa Cruz, CA 95064, USA[22]

C.N. Booth, C.A.J. Brew, S. Cartwright, F. Combley, M.S. Kelly, M. Lehto, J. Reeve, L.F. Thompson

Department of Physics, University of Sheffield, Sheffield S3 7RH, United Kingdom[10]

K. Affholderbach, A. Böhrer, S. Brandt, G. Cowan, C. Grupen, P. Saraiva, L. Smolik, F. Stephan

Fachbereich Physik, Universität Siegen, 57068 Siegen, Fed. Rep. of Germany[16]

M. Apollonio, L. Bosisio, R. Della Marina, G. Giannini, B. Gobbo, G. Musolino

Dipartimento di Fisica, Università di Trieste e INFN Sezione di Trieste, 34127 Trieste, Italy

J. Rothberg, S. Wasserbaech

Experimental Elementary Particle Physics, University of Washington, WA 98195 Seattle, U.S.A.

S.R. Armstrong, E. Charles, P. Elmer, D.P.S. Ferguson, Y. Gao, S. González, T.C. Greening, O.J. Hayes, H. Hu, S. Jin, P.A. McNamara III, J.M. Nachtman,[24] J. Nielsen, W. Orejudos, Y.B. Pan, Y. Saadi, I.J. Scott, J. Walsh, Sau Lan Wu, X. Wu, G. Zobernig

Department of Physics, University of Wisconsin, Madison, WI 53706, USA[11]

[1]Now at CERN, 1211 Geneva 23, Switzerland.
[2]Also at CERN, 1211 Geneva 23, Switzerland.
[3]Also at Dipartimento di Fisica, INFN, Sezione di Catania, Catania, Italy.
[4]Also Istituto di Fisica Generale, Università di Torino, Torino, Italy.
[5]Also Istituto di Cosmo-Geofisica del C.N.R., Torino, Italy.
[6]Supported by the Commission of the European Communities, contract ERBCHBICT941234.
[7]Supported by CICYT, Spain.
[8]Supported by the National Science Foundation of China.
[9]Supported by the Danish Natural Science Research Council.
[10]Supported by the UK Particle Physics and Astronomy Research Council.
[11]Supported by the US Department of Energy, grant DE-FG0295-ER40896.
[12]Permanent address: Kangnung National University, Kangnung, Korea.
[13]Supported by the US Department of Energy, contract DE-FG05-92ER40742.
[14]Supported by the US Department of Energy, contract DE-FC05-85ER250000.
[15]Permanent address: Universitat de Barcelona, 08208 Barcelona, Spain.
[16]Supported by the Bundesministerium für Bildung, Wissenschaft, Forschung und Technologie, Fed. Rep. of Germany.
[17]Supported by the Direction des Sciences de la Matière, C.E.A.
[18]Supported by Fonds zur Förderung der wissenschaftlichen Forschung, Austria.
[19]Also at Istituto di Matematica e Fisica, Università di Sassari, Sassari, Italy.
[20]Now at Schweizerischer Bankverein, Basel, Switzerland.
[21]Now at University of Geneva, 1211 Geneva 4, Switzerland.
[22]Supported by the US Department of Energy, grant DE-FG03-92ER40689.
[23]Now at School of Operations Research and Industrial Engineering, Cornell University, Ithaca, NY 14853-3801, U.S.A.
[24]Now at University of California at Los Angeles (UCLA), Los Angeles, CA 90024, U.S.A.
[25]Now at Harvard University, Cambridge, MA 02138, U.S.A.

1 Introduction

In previous publications by the ALEPH collaboration [1, 2], three-jet events were used to investigate the internal structure of identified quark and gluon jets. Since then, theoretical developments [3] and the availability of additional data have motivated an update and extension of these analyses.

The measurements are based on approximately 3×10^6 hadronic Z decays recorded between 1991 and 1994 by the ALEPH detector [4] at the LEP storage ring, operating at a centre-of-mass energy of $E_{cm} = 91.2$ GeV. From these, 70 000 three-jet events are selected using the Durham clustering algorithm [5] with a jet resolution parameter of $y_{\rm cut} = y_1 = 0.1$. A gluon jet is identified by requiring evidence for long-lived heavy-flavour hadrons in the other two jets; this results in a sample of 4000 gluon jets with a purity of 94.4%. By measuring the properties of all jets in the three-jet sample (consisting of 2/3 quark and 1/3 gluon jets) as well as in the gluon enriched sample, the properties of quark and gluon jets are inferred.

First, distributions of jet-shape variables are considered; these provide a description of the global jet shape. Ranges of the distributions related to hard gluon emission can be identified; here the influences of nonperturbative effects (hadronization) are small, and the predictions of perturbative QCD are expected to be reliable.

Next, the substructure of the jets is investigated. This is done by clustering particles belonging to a jet with a smaller resolution scale ($y_0 < y_1$) than was used for the initial jet selection, so that subjets are resolved. By measuring the means, $\langle N_{\rm q} \rangle$ and $\langle N_{\rm g} \rangle$, and the standard deviations, $\sigma_{\rm q}$ and $\sigma_{\rm g}$, of the subjet multiplicity distribution for quark and gluon jets as a function of the subjet resolution scale y_0, one can study the transition from hard to soft QCD. That is, one can determine a range of subjet scales in which perturbative predictions can be tested, and investigate at what scale nonperturbative effects become large.

The mean subjet multiplicities reported here represent updates of previously published values [1], now based on a larger data sample and with further studies of systematic uncertainties. The standard deviations $\sigma_{\rm g}$ and $\sigma_{\rm q}$ are measured here for the first time. The means and standard deviations are now also measured as a function of jet energy, opening a new degree of freedom for QCD tests.

In the limit of small subjet scales ($y_0 \to 0$), individual particles are resolved. Here the charged particle fragmentation functions for quark and gluon jets are measured. These can be used as input for an investigation of scaling violations of fragmentation functions, as well as providing predictions for jets produced in other processes.

An important feature of the analysis is the choice of a relatively large resolution parameter ($y_1 = 0.1$) to select the three-jet events. This leads to well-separated jets, where the smallest interjet angle is typically greater than 90 degrees. In addition, it is possible to study the internal jet structure up to the scale of $y_1 = 0.1$; this extends well into the range where perturbative predictions are valid.

More details on the measurements presented here can be found in [6, 7].

2 The ALEPH detector

A detailed description of the ALEPH detector can be found in Ref. [4], and an account of its performance as well as a description of the standard analysis algorithms in Ref. [8]. Briefly, the tracking system consists of a silicon vertex detector, a cylindrical drift chamber and a large time projection chamber (TPC), which measures up to 21 three dimensional space points per track.

All these subdetectors are situated in a 1.5 T magnetic field provided by a superconducting solenoidal coil. Between the TPC and the coil, a highly granular electromagnetic calorimeter is used to identify electrons and photons and to measure their energy. The iron return yoke is instrumented to provide a measurement of the hadronic energy and, together with external chambers, muon identification. The measurements presented here are based on charged particle measurements from the tracking chambers as well as information on neutral particles from the electromagnetic and hadronic calorimeters.

In addition to the ALEPH data, simulated events were generated in order to correct for detector effects and to estimate the gluon jet purity of a jet sample. These were produced with the JETSET Monte Carlo model [9], version 7.3. Modifications for radiative effects using the program DYMU3 [10] as well as improved bottom and charm decay tables were included. The important parameters of the generator were tuned to describe ALEPH measurements of charged particle inclusive and event-shape distributions [11]. The generated events were passed through the full detector simulation and reconstruction program.

3 Definition of observables

Jets are defined by means of the Durham clustering algorithm [5]. For each pair of particles i and j the quantity y_{ij} is calculated as

$$y_{ij} \;=\; \frac{2\min(E_i^2, E_j^2)\,(1-\cos\theta_{ij})}{E_{\rm vis}^2}\,, \qquad (1)$$

where E_i and E_j are the particles' energies, θ_{ij} is the angle between the momentum directions, and $E_{\rm vis}$ is the total visible energy in the event. The pair with the smallest value of y_{ij} is found, and if this is below a given resolution parameter $y_{\rm cut}$, then the pair is replaced by a pseudoparticle with four momentum $p^\mu = p_i^\mu + p_j^\mu$ (the "E" recombination scheme). The procedure is then repeated using the new set of particles and pseudoparticles. When all the values of y_{ij} are greater than $y_{\rm cut}$, the clustering procedure stops. Each particle in the event is uniquely associated with a cluster (jet). The algorithm is used to select three-jet events with $y_{\rm cut} = y_1 = 0.1$. The same clustering procedure is also applied further in the definitions of several of the observables.

Distributions of event-shape variables are well established as a useful measure of the global structure of hadronic final states. In a corresponding way, distributions of jet-shape variables allow one to characterize the overall structure of quark and gluon jets.

The jet broadening variable is defined as

$$B_{\rm jet} = \frac{\sum_{i=1}^{N} |p_\perp^i|}{\sum_{i=1}^{N} |p^i|}\,.$$

Here $p_\perp^i$ is the momentum of particle i transverse to the jet axis, and the sum extends over all of the N particles in the jet. The variable here is analogous to the quantities wide and narrow jet broadening, which are defined for particles in separate hemispheres of an event [12].

Another jet-shape variable called y_2 (also referred to as the differential one-subjet rate) is defined by clustering the particles in a jet until two clusters (subjets) result. The value of y_2 is then given by the Durham scale (1) between the two subjets. By construction this can vary from zero up to the jet resolution parameter y_1. The integral of the distribution from a given value of y_2 up to y_1 corresponds to the probability for a parton to split into two further partons which

are resolved at a scale y_2. For reasons of convenience, the distributions are in fact presented using the equivalent variable $L_2 = -\ln y_2$.

In order to investigate the internal jet structure, the particles of the individual jets are clustered using again the Durham algorithm, where the quantity y_{ij} (1) is still normalized using the visible energy of the entire event. Now, however, a subjet resolution scale y_0 less than y_1 is used, so that subjets are resolved. The mean values, $\langle N_{\mathrm{g}} - 1\rangle$ and $\langle N_{\mathrm{q}} - 1\rangle$, and the standard deviations, σ_{g} and σ_{q}, of the subjet multiplicity distributions for gluon and quark jets are then measured as a function of y_0. In addition, the ratios

$$R_N(y_0) = \frac{\langle N_{\mathrm{g}}(y_0) - 1\rangle}{\langle N_{\mathrm{q}}(y_0) - 1\rangle}\,, \qquad R_\sigma(y_0) = \frac{\sigma_{\mathrm{g}}(y_0)}{\sigma_{\mathrm{q}}(y_0)}\,,$$

are determined. The quantities $\langle N_{\mathrm{g}} - 1\rangle$ and $\langle N_{\mathrm{q}} - 1\rangle$ are directly related to the probability for additional partons to be emitted from the original gluon or quark. This definition results in a simple expression for the perturbative QCD prediction at leading-log accuracy for R_N of $C_A/C_F = 9/4$, valid for all values of y_0. For sufficiently large y_0, corresponding to a sufficiently large transverse momentum separation between subjets, one expects that perturbative predictions should be valid and that the subjets should thus reflect the underlying partonic structure of the event. By going to smaller values of y_0 one can investigate the extent to which the perturbative predictions remain valid and determine scales where nonperturbative effects become important.

In the limit of small subjet scales ($y_0 \to 0$), individual particles are resolved. From these, the distributions (fragmentation functions) of $x = E_{\mathrm{hadron}}/E_{\mathrm{jet}}$ have been measured for charged particles in quark and gluon jets.

4 Analysis procedure

The analysis procedure is essentially the same as in the previous ALEPH publication on subjets [1]. Here only the basic features are described.

Hadronic events are selected by requiring at least 5 well reconstructed tracks and a total energy for charged particles (assuming the pion rest mass) of at least 10% of the centre-of-mass energy. It is also required that the total visible energy be at least 20 GeV. This results in a sample of approximately 3 million hadronic events.

Three-jet events are selected with a jet resolution parameter of $y_{\mathrm{cut}} = y_1 = 0.1$. To reject events of the type $q\bar{q}\gamma$, an event is not accepted if more than 85% of the energy of a jet is carried by a single photon. In order to ensure that most of the particles of a jet pass through the vertex detector, it is required that each jet have an angle of at least 35° with respect to the beam axis. This selection results in a sample of about 70 000 three-jet events, with no significant background from other event types such as $\tau^+\tau^-$ final states or two-photon collisions.

From the three-jet events, two samples of jets are obtained, each with different relative fractions of quark and gluon jets. One sample consists of all the jets in the selected three-jet events. This *mixed* sample ($\approx$ 210 000 jets) contains about 1/3 gluon and 2/3 quark jets. (In fact, a gluon jet fraction of 32.7% is estimated from the Monte Carlo; this differs from 1/3 because of ambiguous events where both primary quarks are clustered into the same jet.) A second sample highly enriched in gluon jets is obtained by requiring evidence of long-lived heavy-flavour hadrons in two of the three jets. The technique for identifying heavy-quark jets is based on a three-dimensional impact parameter measured for each charged-particle track [13]. The

two heavy-quark jets are rejected and the third is taken as a gluon jet candidate. This results in about 4 000 jets (the *tagged* sample) with a gluon jet purity of $(94.4 \pm 0.3(\text{stat.}))\%$

A two-step correction procedure is used to determine the distributions for pure samples of quark and gluon jets. First, the distributions for the mixed and tagged samples are corrected for detector effects such as finite acceptance and resolution, initial state photon radiation (ISR) and biases introduced by the analysis method (e.g. tagging). Then an unfolding procedure is applied to relate the corrected distributions for the mixed and tagged samples to those of pure quark and gluon jets. Details can be found in reference [1]. For the quantities determined as a function of jet energy, the gluon-jet purities used in the correction and unfolding procedures must be determined as a function of E_{jet}.

Because of the larger data sample compared to that used in the previous ALEPH publication on subjets, possible sources of systematic uncertainties were investigated in greater detail. The following sources of uncertainty were found to be important. First, the correction factors derived from the Monte Carlo, which are used to correct the observables for detector effects, could have a dependence on the event generator used. This was investigated by computing correction factors with a simplified, fast detector simulation and using the generators JETSET 7.4 [9], HERWIG 5.8 [14] and ARIADNE 4.06 [15]. The maximum variation in the results was included in the systematic error. In addition, the accuracy of the detector simulation was investigated by successively varying the analysis cuts and repeating the analysis. The largest changes in results relative to those based on standard cuts come from the following variations: (a) minimum energy required for neutral particles, (b) minimum angle required between jet axis and beam axis in order to measure the complete jet in the detector, (c) the selection cut for identifying gluon jet candidates.

The total systematic error is obtained by adding the uncertainty from the detector correction factors and the three sources from the detector simulation in quadrature. The relative sizes of these contributions differ from observable to observable and also vary over the measured range of a given observable. As a general rule, the total systematic error is comparable to the statistical error.

5 Results

In the following sections the measurements are presented and compared to predictions of perturbative QCD and Monte Carlo models. The important parameters of the models were tuned to describe ALEPH measurements of charged particle inclusive and event-shape distributions [16]. The error bars on the plots show the quadratic sum of statistical and systematic uncertainties.

Most of the observables considered here are integrated over jet energies and interjet angles. Only for the mean and width of the subjet multiplicity distribution are the data also investigated in bins of jet energy (in that case the observables are still integrated over interjet angles). Because of the large jet-resolution parameter used ($y_1 = 0.1$), the smallest interjet angle is always greater than 60 degrees, with the most probable value being around 100 degrees. Distributions of jet energies and the smallest interjet angle can be found in [1].

5.1 Jet-shape variables

The measured B_{jet} distribution is shown in Fig. 1 along with the predictions of the Monte Carlo models JETSET, HERWIG and ARIADNE. The measured values are given in Table 1. In

general, the models describe the data reasonably well. There is good agreement in the regions of large $B_{\rm jet}$, where hadronization corrections are small and the distributions are sensitive to perturbative physics. This was investigated with the JETSET model by comparing the $B_{\rm jet}$ distributions at parton and hadron level. As can be seen in Fig. 2(a), hadronization effects are negligible at large $B_{\rm jet}$.

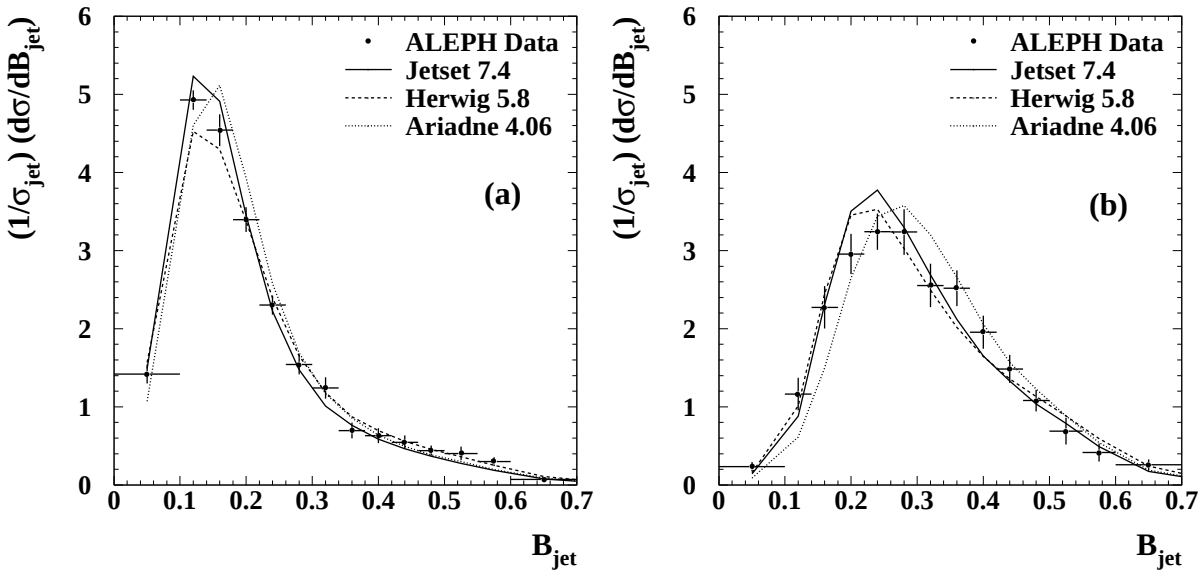

Figure 1: The measured $B_{\rm jet}$ distribution for (a) quark and (b) gluon jets in comparison with Monte Carlo models.

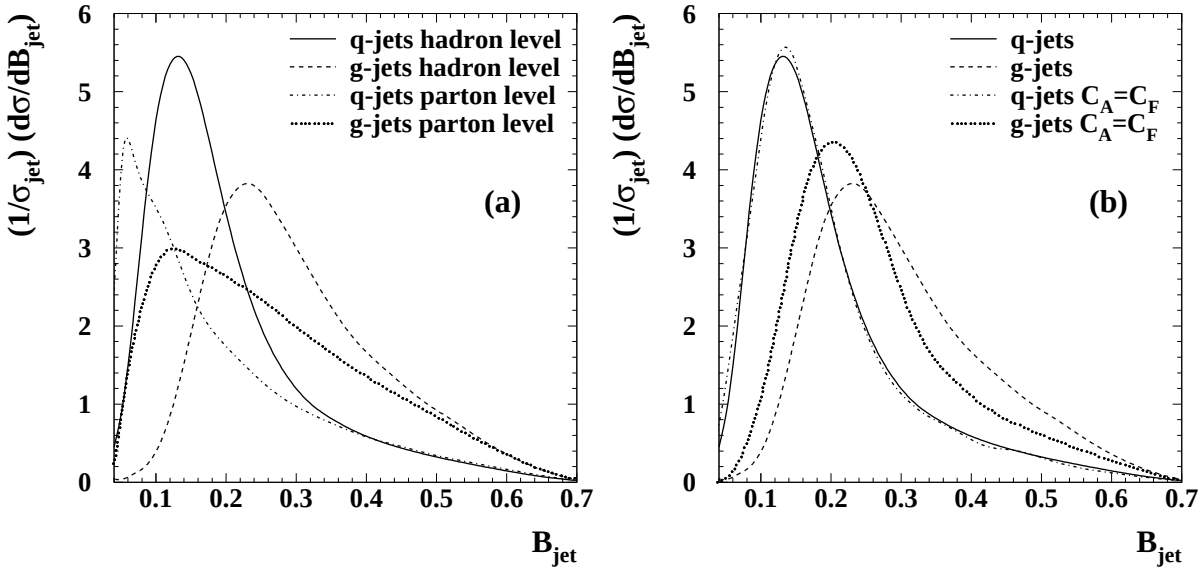

Figure 2: The $B_{\rm jet}$ distribution predicted by the JETSET 7.4 Monte Carlo (a) comparing hadron and parton level distributions, and (b) comparing hadron level distributions with different couplings for the parton splitting $g \to gg$ (see text).

In order to investigate whether the distribution is sensitive to perturbative physics, the effective coupling of the splitting $g \to gg$ was changed from its QCD value $C_A\alpha_s$ to $C_F\alpha_s$ (where $C_A = 3$ and $C_F = 4/3$), which is the corresponding value for $q \to qg$. The resulting hadron-level distributions are shown in Fig. 2(b). The quark-jet distribution remains largely unchanged, whereas the distribution for gluon jets is suppressed at large $B_{\rm jet}$. A large part of the difference between quark and gluon jets is thus seen to stem from the higher effective colour charge of the gluon predicted by QCD, rather than being, for example, a simple consequence of kinematics. Similar results are found for the y_2 distribution.

Figure 3 shows the measured y_2 distribution for quark and gluon jets along with the predictions of Monte Carlo models and also from leading order (LO) QCD [17] without any modifications for hadronization. The measured values are given in Table 2. The LO prediction is expected to be valid only in the region of large y_2 (small $L_2 = -\ln y_2$) where hard emission dominates and hence the effects of higher orders should be small. For small y_2 emission of soft and collinear partons becomes important. In fact, the prediction shows significant discrepancies with the data already for L_2 above 3.5 (y_2 below 0.03). Monte Carlo studies with the y_2 distribution lead to similar conclusions concerning sensitivity to hadronization and perturbative effects in the region of large y_2 as was seen for large $B_{\rm jet}$.

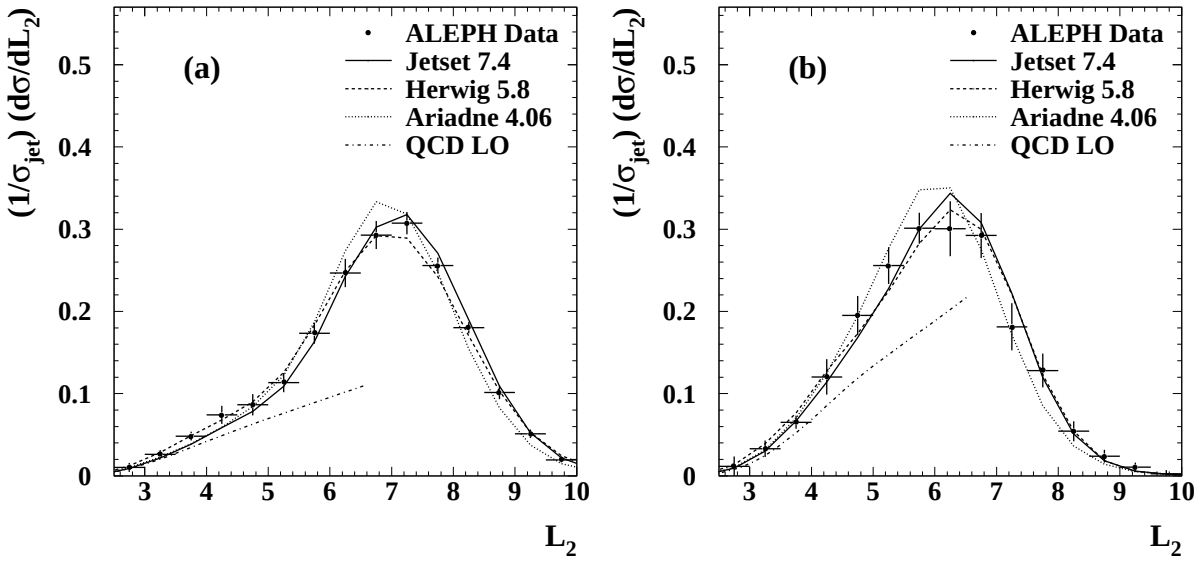

Figure 3: The measured $L_2 = -\ln y_2$ distribution for (a) quark and (b) gluon jets compared to the predictions of Monte Carlo models. The dashed-dotted curve shows the leading-order QCD prediction.

5.2 Subjet structure without consideration of jet energy

First the properties of the subjet multiplicity distribution are examined without consideration of the jet energy. Various properties are shown as a function of the resolution parameter y_0 in Fig. 4 along with the predictions of the JETSET, HERWIG and ARIADNE models. Figures 4 (a) and (b) show the mean subjet multiplicity minus one for gluon and quark jets, and (c) shows their ratio R_N. The standard deviations $\sigma_{\rm g}$ and $\sigma_{\rm q}$ and their ratio R_σ are shown in Figs. 4 (d) – (f). These results are also given in Tables 3 and 4, together with their statistical and systematic uncertainties.

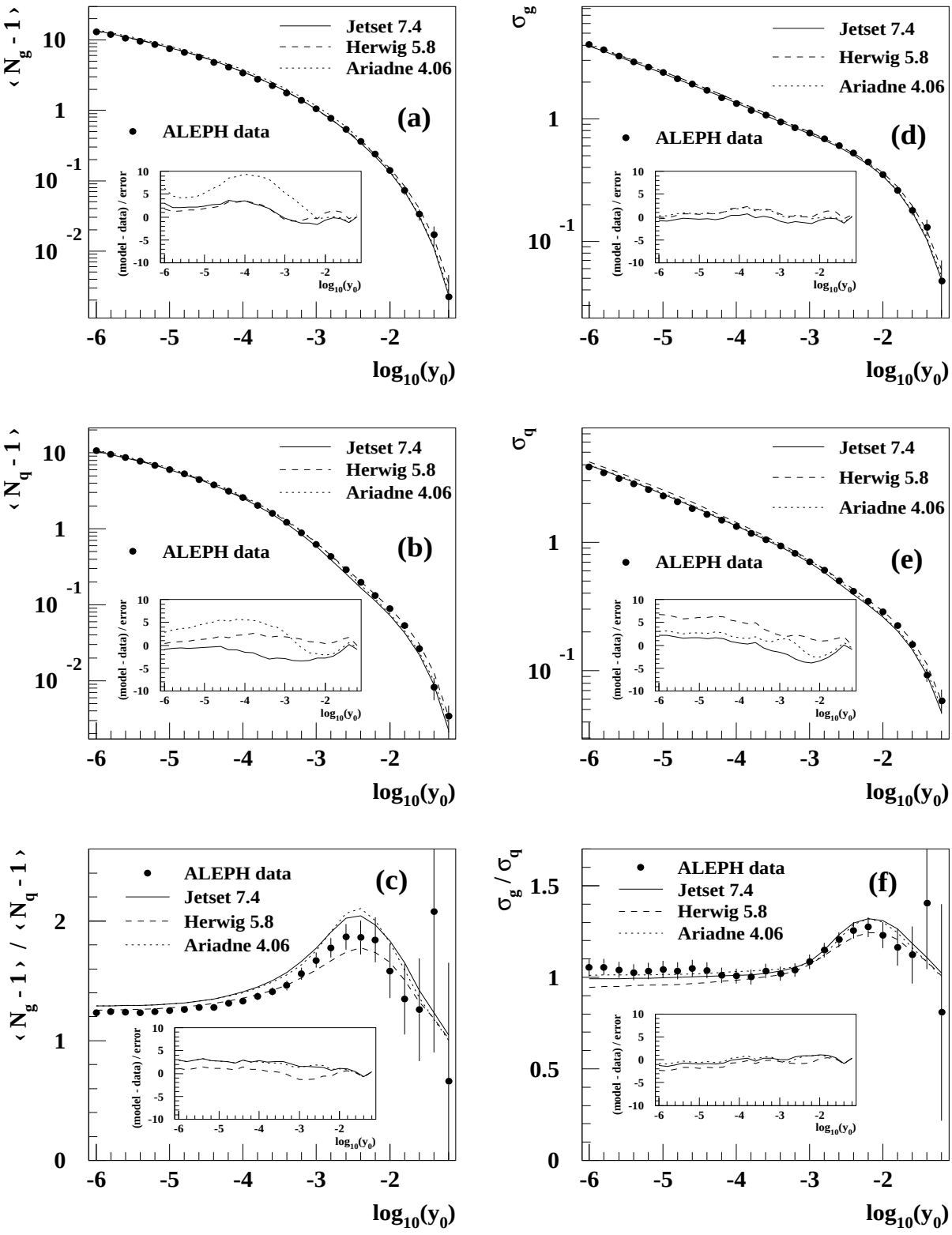

Figure 4: The mean (left-hand side) and the width (right-hand side) of the subjet multiplicity distribution are shown for gluon jets, quark jets and the ratio $\frac{gluon}{quark}$ as a function of the subjet resolution parameter y_0. The full dots show the measurement and the different lines represent the predictions of MC models. The inset plots show the deviations of the model predictions from the data divided by the total error. All plots apply to the whole interval of available jet energies.

The agreement with the Monte Carlo models is seen to be qualitatively good, especially when one considers that the observables vary over several orders of magnitude within the range studied. For the mean subjet multiplicities, this confirms the observations in [1], now at a sufficiently high level of precision to discriminate between models. For the multiplicities $\langle N_{\rm g} - 1 \rangle$, $\langle N_{\rm q} - 1 \rangle$ and their ratio R_N, HERWIG is seen to give the best description.

From the inset plots one can also see that the predicted multiplicities from ARIADNE are high for both quark and gluon jets. Although the discrepancy is small in absolute terms, it is significant compared to the size of the errors, which are $1 - 2$ % for $y_0 < 10^{-3}$. Results for neighbouring values of y_0, however, are highly correlated.

For the standard deviations and their ratio, the picture is somewhat different. There, all models provide a good description of the gluon jets. For the quark jets, however, HERWIG predicts a too broad subjet multiplicity distribution at small y_0. This observation is of particular interest, since previous measurements had shown that HERWIG's prediction for the width of the charged particle multiplicity distribution for entire events was also significantly too large [16, 18]. This discrepancy is now seen to stem from the quark jets only.

In Fig. 5, the same results are compared with perturbative QCD predictions without any modifications for hadronization effects [3], as well as with the hadron- and parton-level predictions of the JETSET model. From the comparison of the hadron and parton levels of JETSET for the observables $\langle N_{\rm g} - 1 \rangle$, $\langle N_{\rm q} - 1 \rangle$, $\sigma_{\rm g}$, and $\sigma_{\rm q}$, one can see that the effects of hadronization are small as long as y_0 is sufficiently large. This range of y_0 values ($y_0 > 10^{-3}$) will be referred to as the perturbative region. For small y_0, hadronization effects are seen to become large. The parton level in the Monte Carlo model is not, however, calculated to the same level of accuracy as the QCD predictions discussed below.

Perturbative QCD predictions for $\langle N_{\rm g} - 1 \rangle$ and $\langle N_{\rm q} - 1 \rangle$ can be obtained to leading order (LO) in α_s with the $O(\alpha_s^2)$ matrix element. (One order of α_s is necessary to produce a three-jet event.) The LO result can be improved by combining it with the resummation of leading and next-to-leading logarithmic terms in y_1/y_0 to all orders in α_s (LO+NLLA). The LO and LO+NLLA predictions and the estimate of the theoretical uncertainty for the resummed result (shown as a hatched area between two lines in Figs. 5(a)–(c)) are taken from [3].

From Figs. 5(a) and (b), one can see that the LO prediction is compatible with the data only at very high values of y_0. A better description, extending to around $y_0 \approx 10^{-3}$ for both quark and gluon jets, is given by the parton level predictions of JETSET. Further improvement is obtained with the LO+NLLA prediction. For $10^{-5} < y_0 < 10^{-3}$, the difference between data and prediction is less than around 20% for gluon jets but is more than 50% for quark jets. The larger discrepancy for quark jets has been shown by Monte Carlo studies to result from quark mass and hadronization effects. In fact these studies show that the fall-off of R_N at small y_0 is due partly to the higher multiplicity b-quark jets, which start to exert their influence for decreasing y_0 at around $y_0 \sim 10^{-2.6}$.

Resumming the logarithms of y_1/y_0 has roughly the same influence on both $\langle N_{\rm g} - 1 \rangle$ and $\langle N_{\rm q} - 1 \rangle$, so that this has little influence on R_N, i.e. the LO and LO + NLLA predictions for R_N are very similar. If only the leading-log contributions (LLA) are considered, the QCD prediction for the ratio R_N is given by the ratio of colour factors $R_N = C_A/C_F = 9/4$, independent of y_0. Including the fixed order (LO) calculation not only lowers the prediction, bringing it in closer agreement with the data, but also provides qualitatively the correct y_0 dependence for large y_0 (cf. Fig. 5(c)).

The plot of the ratio R_N in Fig. 5(c) also shows the hadron level prediction of a JETSET-based Monte Carlo where the effective coupling for the branching $g \to gg$ was changed from

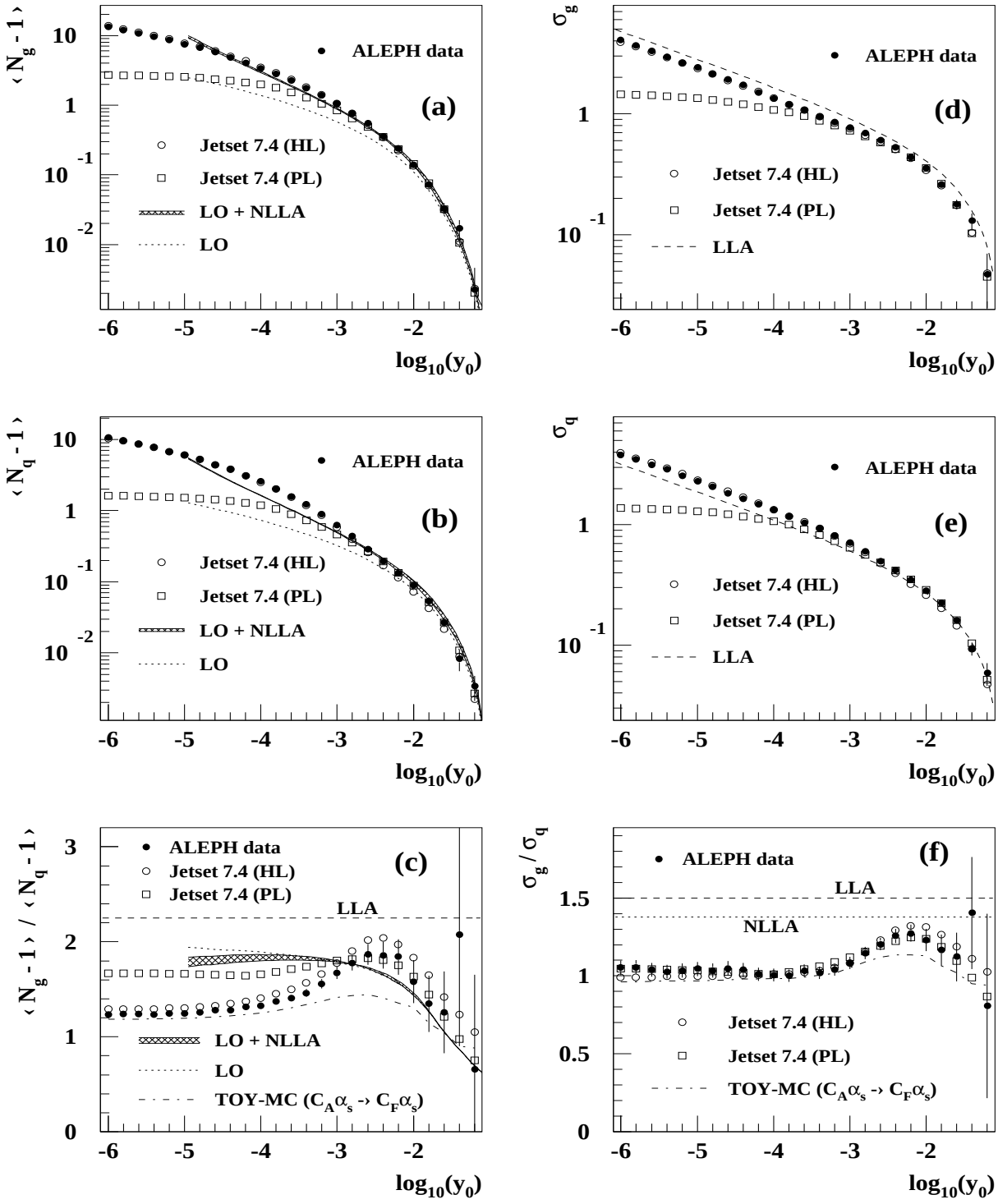

Figure 5: The mean (left-hand side) and the width (right-hand side) of the subjet multiplicity distribution are shown for gluon jets, quark jets and the ratio $\frac{gluon}{quark}$ as a function of the subjet resolution parameter y_0. The full dots show the measurement and the open circles and squares represent the hadron and parton level from the JETSET MC (if the open circles are not visible in some of the plots they lie on top of the data points). The dashed-dotted line in the ratio plots shows the hadron level prediction of JETSET with $C_A\alpha_s$ changed to $C_F\alpha_s$ (see Section 5.1). The other lines show perturbative QCD predictions at various levels of precision (see text).

$C_A\alpha_s$ to $C_F\alpha_s$ (cf. Section 5.1). In the region where hadronization effects are expected to be small ($10^{-3} < y_0 < 10^{-2}$), the ratio R_N from the modified JETSET is around $1.3 - 1.4$, whereas for the standard JETSET model it is predicted to rise to around 2. This indicates that one is sensitive to perturbative effects. For smaller y_0, however, the standard and modified models give similar predictions, indicating that here R_N is not sensitive to the effective colour charge in the parton shower.

The comparison of QCD predictions and mean subjet multiplicities will be considered further in Section 5.3, where measurements of $\langle N_{\rm g} - 1\rangle$ and $\langle N_{\rm q} - 1\rangle$ will be used to determine QCD parameters.

For the standard deviations, $\sigma_{\rm g}(y_0)$ and $\sigma_{\rm q}(y_0)$, the analytical prediction as a function of y_0 is only available in leading-log accuracy [19, 20]. The y_0 dependence for both quantities is the same, and hence the prediction for the ratio is a constant. This is given by the square root of the ratio of colour factors $R_\sigma = \sqrt{C_A/C_F} = 3/2$ [20]. For the ratio R_σ, a prediction in next-to-leading log approximation is also available [21]. In both leading and next-to-leading log accuracy, R_σ is predicted to be greater than one, i.e. gluon jets should have a broader multiplicity distribution than quark jets. Other QCD calculations [22], however, have led to predictions of R_σ less than one, which is in disagreement with the data in the perturbative region.

The standard deviations $\sigma_{\rm g}$ and $\sigma_{\rm q}$ are in qualitatively good agreement with the LLA prediction. The agreement may in fact be better than expected, since these quantities should be sensitive to next-to-next-to-leading logarithmic terms in y_1/y_0 [23]. Although the y_0 dependence of $\sigma_{\rm g}$ and $\sigma_{\rm q}$ are well reproduced, one can see that the overall normalization of the LLA curves is not correctly predicted. The LLA predictions depend on an effective strong coupling constant $\alpha_s^{\rm LLA}$; by varying this one can obtain better agreement with the data for gluon jets ($\alpha_s^{\rm LLA} \approx 0.09$) or for quark jets ($\alpha_s^{\rm LLA} \approx 0.15$), but not simultaneously for both. This suggests that higher order corrections should primarily affect the relative normalization of the gluon and quark jet curves.

In fact, the next-to-leading log prediction for R_σ shows better agreement with the data than the LLA in the perturbative region near $y_0 \simeq 10^{-2}$ (see Fig. 5(f)). In principle, calculations based on resummation of logarithms of y_1/y_0 should be most reliable for small y_0 (i.e. large logarithms). In this limit, however, hadronization effects for $\sigma_{\rm g}$ and $\sigma_{\rm q}$ are large, and indeed one sees that the agreement with the data for R_σ is poor. The measured R_σ at small y_0 is approximately 1, so that here no significant difference between quark and gluon jets is visible. In the perturbative region around $y_0 \simeq 10^{-2}$, the hadronization effects are relatively small and $\ln y_1/y_0 \approx 2$ to 3 is sufficiently large that the resummed prediction is valid. These considerations on the region of validity of the resummed prediction for R_σ are correspondingly valid for the ratio R_N.

The decrease of $R_N(y_0)$ and $R_\sigma(y_0)$ for $y_0 \to y_1$ seen in Figs. 4 and 5 can at least partly be explained by the difference in the mean gluon and quark jet energies. The mean gluon jet energy is measured to be 14% lower than the mean quark jet energy. Since it is possible to resolve an additional subjet at the scale $y_0 \lesssim y_1$ only for very high energy jets, this is more likely to be the case for quark jets, and therefore the ratio R_N is suppressed. This effect can be explored further by measuring the properties of the subjet multiplicity distribution for jets in a specific bin of jet energy, as done in Section 5.4.

5.3 QCD parameters from subjet multiplicities

In this section, the QCD colour factor C_A, which corresponds to the vertex $g \to gg$, is treated as an effective free parameter and is determined using the measurement of $\langle N_{\rm g} - 1\rangle(y_0)$ and

$\langle N_{\rm q}-1\rangle(y_0)$. The extent to which one obtains the QCD value, $C_A = 3$, then serves to quantify the agreement between the measurement and the LO+NLLA prediction and shows the sensitivity of $\langle N_{\rm g}-1\rangle(y_0)$ and $\langle N_{\rm q}-1\rangle(y_0)$ to perturbatively calculable effects. Since there is a strong correlation between the results for neighbouring values of the subjet resolution parameter y_0, which is difficult to estimate in detail, C_A is determined independently for three different values of y_0: $10^{-3.2}$, $10^{-2.6}$, and $10^{-2.0}$; these correspond to transverse energies of $k_t = E_{\rm cm}\sqrt{y_0} \approx 2.3\,\mathrm{GeV}$, 4.6 GeV, and 9.1 GeV, respectively.

Because the theoretical prediction used is only complete to leading order in α_s, the renormalization scheme is not fixed. Therefore α_s cannot be identified with values determined in the $\overline{MS}$ scheme and must be understood as an effective parameter, in the following called $\alpha_s^{\rm eff}$. Its value therefore cannot be taken from other measurements but rather it must be determined simultaneously with C_A. The accuracy for C_A obtained here is less than that achieved in analyses of angular variables in four-jet events (see e.g. [24, 25, 26]). Nevertheless, the measurement here is of interest because of the direct connection between the colour factor and the observable in question, since the subjet multiplicity is closely related to the probability for a parton to branch into two partons.

To compare the QCD prediction with the measurement, the perturbative calculation has to be modified for effects of hadronization. This is done by means of multiplicative correction factors derived from the Monte Carlo models JETSET, HERWIG and ARIADNE. The final correction factor used is taken as the average of the corrections derived from the three models.

Systematic errors are determined taking into account the correlation between the quark and gluon jet measurements. Sources of systematic errors are explained in Section 4, and contain in addition the uncertainties of the hadronization corrections and of the perturbative prediction. The latter is estimated by using two different scales to calculate the resummed result [3]. The uncertainty of the hadronization corrections is estimated from the difference in the fit results when using only the JETSET, HERWIG, or ARIADNE hadronization corrections. Additional systematic uncertainty comes from a possible QCD parameter dependence of the hadronization corrections. This is found to be of about the same size as the uncertainty due to the variation of the Monte Carlo model to calculate the hadronization corrections. It was also checked that the cut-off parameter for the parton shower in the different models has a negligible influence on the results.

Since only two observables are used as input, ($\langle N_{\rm g}-1\rangle$ and $\langle N_{\rm q}-1\rangle$ at a fixed value of y_0), there are zero degrees of freedom and one solves for $\alpha_s^{\rm eff}$ and C_A rather than fitting them. Nevertheless, confidence limits can be obtained in the plane of $\alpha_s^{\rm eff}$ and C_A. The other QCD colour factors corresponding to the vertices $q \to qg$ and $g \to q\overline{q}$, are fixed to their nominal QCD values, $C_F = 4/3$ and $T_R = 0.5$. The effective number of flavours is set to $N_f = 5$.

Figure 6 shows the 68.3 % confidence level contours for the three different choices of y_0. The contours include statistical and systematic errors; the systematics dominate for the two lower values of y_0. The results are consistent with each other and are in good agreement with the predicted value of $C_A = 3$. For $y_0 = 10^{-3.2}$, one obtains $C_A = 2.63 \pm 0.10(\mathrm{stat.}) \pm 0.27(\mathrm{sys.})$ and $\alpha_s^{\rm eff} = 0.130 \pm 0.005(\mathrm{stat.}) \pm 0.014(\mathrm{sys.})$ with a correlation coefficient of $\rho = -0.89$.

When all the QCD colour factors are fixed at their standard model values and only the effective strong coupling constant is fitted, one obtains, depending on the y_0 used, values of $\alpha_s^{\rm eff}$ between 0.113 and 0.124. The relative total errors from the sources discussed above are about 5%. This good agreement with the world average value ($\overline{MS}$ scheme) of $\alpha_s(M_{\rm Z}^2) = 0.118 \pm 0.003$ [27] can be attributed to the resummed logarithms in the LO+NLLA prediction used, since pure LO predictions tend to require significantly larger values of α_s to describe the data.

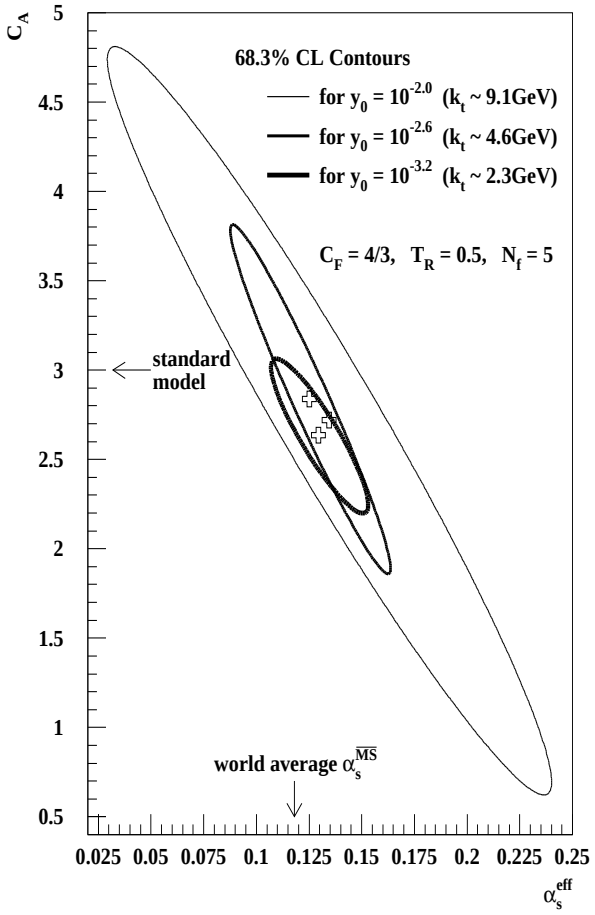

Figure 6: The 68.3 % confidence level contours of the simultaneous determination of C_A and $\alpha_s^{\rm eff}$ for three different values of the subjet resolution parameter: $y_0 = 10^{-3.2}$, $y_0 = 10^{-2.6}$, and $y_0 = 10^{-2.0}$. The error ellipses include statistical and systematic uncertainties.

The branching $g \to q\overline{q}$ is suppressed relative to $g \to gg$, and hence the internal structure of the jets is less sensitive to the colour factor T_R than to C_A. The picture is further complicated by theoretical uncertainties in the number of active quark flavours for a certain choice of y_0 (e.g. production of $b\overline{b}$ pairs is suppressed for small transverse momentum scales). A similar measurement of T_R resulted in large uncertainties and is not shown.

5.4 Subjet structure as a function of jet energy

In this section, the properties of the subjet multiplicity distribution are examined for samples of jets having approximately the same energy. In principle one could measure the subjet properties binned in $E_{\rm jet}$ and also according to the interjet angles, i.e. according to the event topology. Such a study has been carried out for particle multiplicities using a three-jet resolution parameter of $y_{\rm cut} = 0.01$ [28]. Because of the larger resolution parameter used here ($y_{\rm cut} = 0.1$), the sample of three-jet events is not sufficiently large to allow for binning in both energy and angle, and only the energy dependence is investigated. In fact, because of the large $y_{\rm cut}$, fixing the jet energy strongly restricts the allowed interjet angles and thus one would not gain much additional information from the remaining angular dependence.

When the subjet properties are studied for a restricted interval of jet energies, the dependence on y_0 and the level of agreement with Monte Carlo models are qualitatively similar to what was seen in the energy-integrated case. Effects caused by the mean energy difference between quark and gluon jets, however, are now largely removed. This results in a larger rise in the ratios R_N and R_σ for y_0 in the perturbative region, and in a less pronounced fall off for $y_0 \to y_1$. This can be seen from Figs. 7(a) and 7(b), which show the ratios for jets in the energy range $24\,\mathrm{GeV} \leq \mathrm{E_{jet}} \leq 28\,\mathrm{GeV}$ (compare with the energy-integrated case shown in Fig. 4(c) and 4(f)). When E_{jet} is restricted, perturbative QCD predictions are only available for the mean subjet multiplicities. A comparison (not shown) of this with the data leads to similar conclusions as those drawn in Section 5.2.

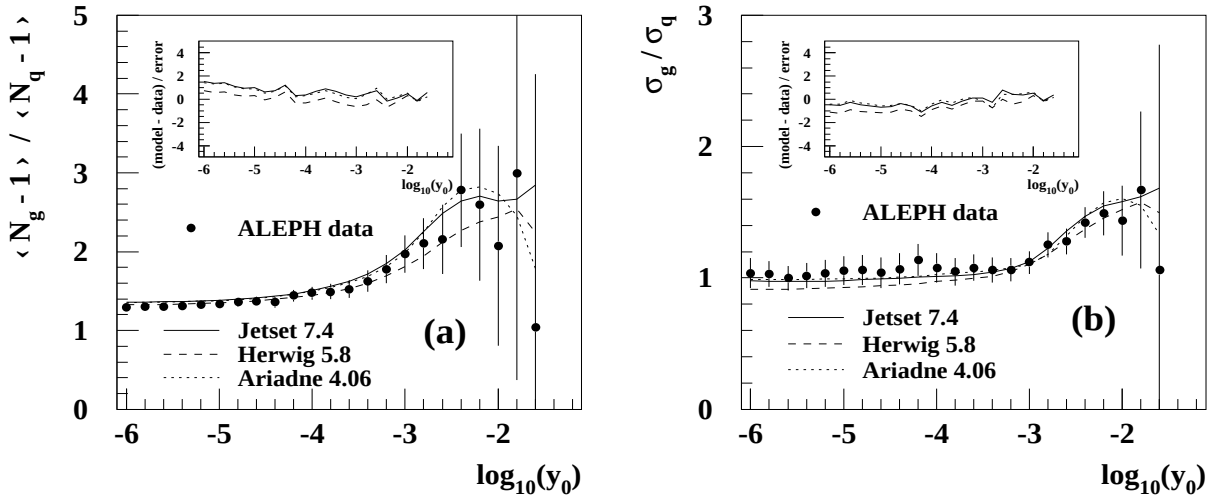

Figure 7: The ratios R_N and R_σ of the means and widths of the subjet multiplicity distributions for gluon and quark jets. The two plots include only jets with an energy in the range $24\,\mathrm{GeV} \leq \mathrm{E_{jet}} \leq 28\,\mathrm{GeV}$. The points show the measurement and the lines are the predictions of Monte Carlo models. The inset plots show the deviations of the model predictions from the data divided by the total error.

The larger rise in the ratios R_N and R_σ compared to the energy-integrated case can be understood by looking at the mean subjet multiplicities and standard deviations as a function of E_{jet} for a fixed value of $y_0 = 10^{-2.2}$ (corresponding to a transverse energy separation between subjets of $k_t = E_{\mathrm{cm}}\sqrt{y_0} \approx 7.2$ GeV), as shown in Fig. 8. The value of y_0 was chosen to be in the region where one is sensitive to perturbative effects and where hadronization effects are relatively small. From Fig. 8 one can see that the multiplicities and standard deviations increase as a function of E_{jet}. If the ratios R_N and R_σ from the energy integrated jet samples are considered, one compares gluon jets with a mean energy of 26.2 GeV with quark jets having a mean energy of 30.4 GeV. Therefore, this results in a lower ratio than in the case where jets of equal energies are compared. Measurements at other y_0 values show a similar dependence on E_{jet}.

While $\langle N_{\mathrm{g}} - 1 \rangle$ steadily increases with increasing jet energy, $\langle N_{\mathrm{q}} - 1 \rangle$ first shows a gentle rise and then, from about $E_{\mathrm{jet}} = 40\,\mathrm{GeV}$ on, increases sharply (cf. Figs. 8(a) and (b)). As a result, R_N shows a clear E_{jet} dependence, first increasing, and then decreasing sharply to approximately 1.0 at $E_{\mathrm{jet}} \approx 40\,\mathrm{GeV}$. This behaviour can be explained by the fact that jets with very high energies often also have a high invariant mass; this is a consequence of four-momentum conservation for the three-jet event. The effect is well predicted by all of the Monte Carlo models considered. Similar considerations also hold for the standard deviations σ_{q}, σ_{g} and their ratio

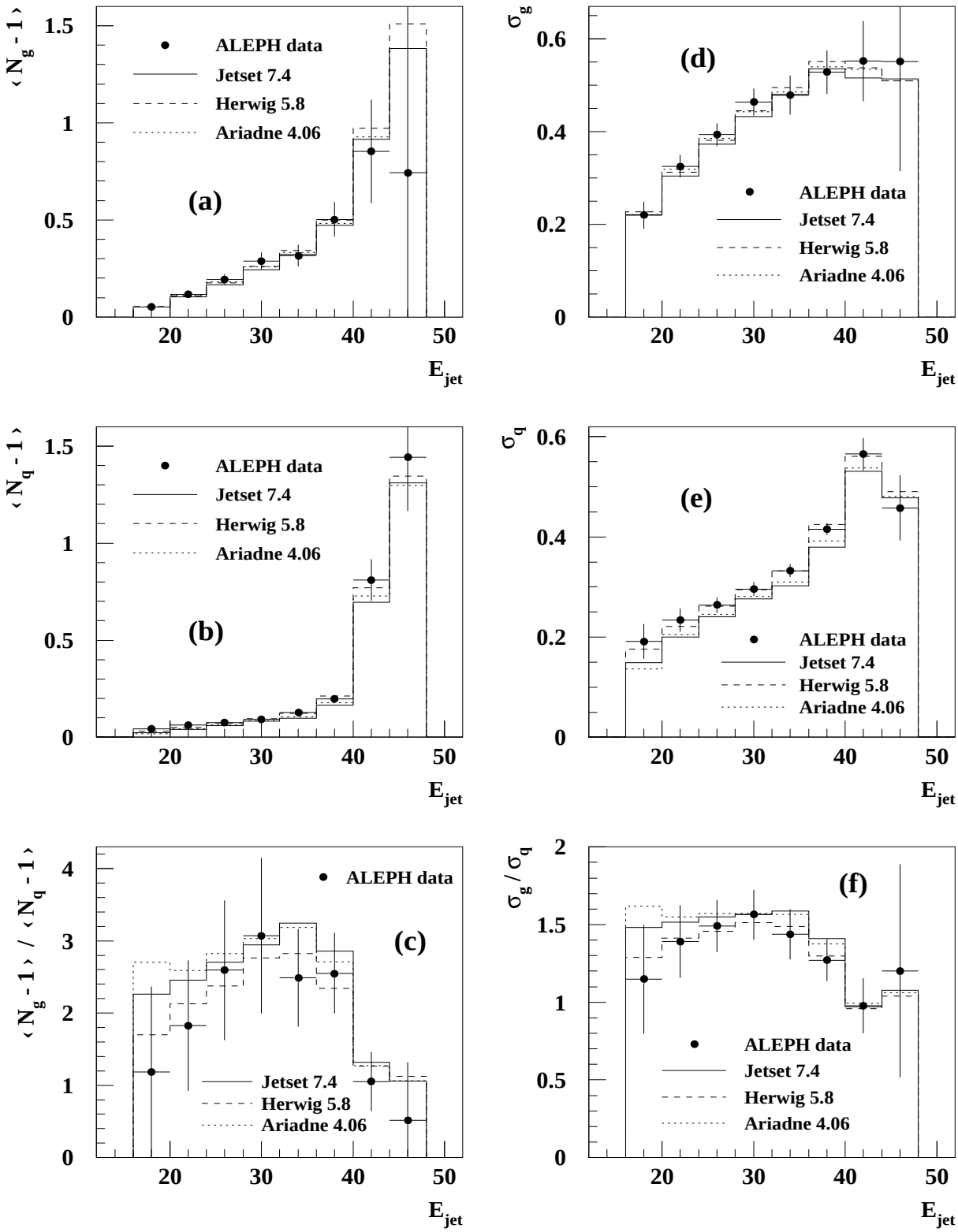

Figure 8: The mean (left-hand side) and the width (right-hand side) of the subjet multiplicity distribution for gluon and quark jets, as well as the ratios R_N and R_σ for fixed $y_0 = 10^{-2.2}$ as a function of $E_{\rm jet}$. The points show the measurement and the curves show the predictions of Monte Carlo models.

R_σ. In particular, R_σ is found to drop to around one for $E_{\rm jet} > 40$ GeV.

5.5 Fragmentation function for charged particles

Figure 9 shows the measured inclusive distribution of $x = E_{\rm hadron}/E_{\rm jet}$ (the fragmentation function) for charged particles in quark and gluon jets along with the predictions of Monte Carlo models. Here the jet energies were estimated from the angles between the three jets using the kinematic relation for massless jets, which improves the jet-energy resolution. While all models describe the spectrum for quark jets quite well, the fragmentation function for gluon jets is predicted softer than measured. As has been observed before [2, 29], this discrepancy is greatest for the HERWIG model. The measurements are also given in Table 5, together with their statistical and systematic uncertainties.

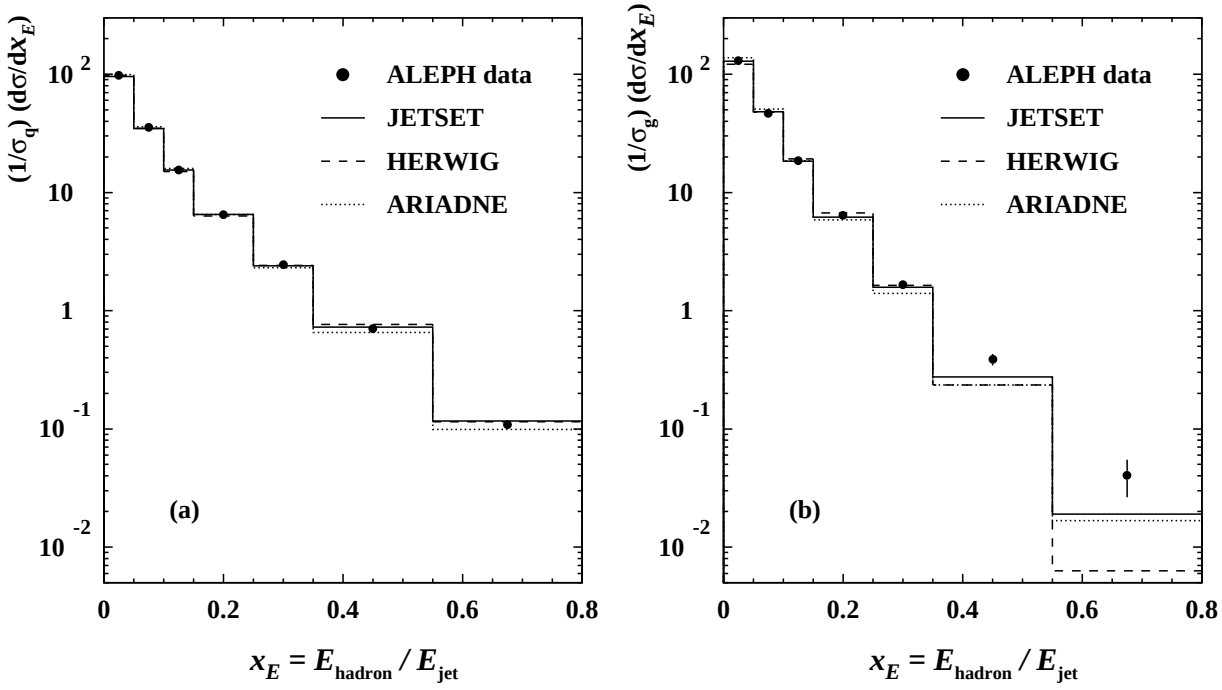

Figure 9: The measured fragmentation function for (a) quark and (b) gluon jets along with the predictions of Monte Carlo models.

Because the effective coupling for $g \to gg$ is larger than that of $q \to qg$, gluon jets are expected to have higher multiplicities and therefore a softer fragmentation function than quark jets. This is in fact observed. Although the exact forms of the fragmentation functions cannot be calculated using perturbative QCD, their energy dependence can be predicted by the DGLAP evolution equations [30]. The measured distributions presented here can be used as input for an investigation of this energy dependence (scaling violations) as was done, for example, in [31].

The measurements presented here are of similar but slightly different observables than the fragmentation functions previously reported by LEP experiments [2, 29]. These measurements were based on jets selected with a resolution parameter of $y_{\rm cut} = 0.01 - 0.02$, and included additional cuts on jet energies and angles. Nonperturbative corrections to the evolution equations for fully inclusive fragmentation functions (i.e. without jet finding) are expected to decrease as $1/E_{\rm cm}$ or faster (see e.g. [32]). If one assumes that a similar dependence holds for

fragmentation functions of jets with a scale $Q = \sqrt{y_{\rm cut}} E_{\rm cm}$, then nonperturbative effects are significantly reduced by using the higher $y_{\rm cut}$. In addition, the measurements here have smaller uncertainties, owing mainly to the large data sample and high gluon jet purity. The present measurements thus provide a more accurate basis for predicting properties of jets in the energy range of the Large Hadron Collider ($10^2 - 10^3$ GeV).

6 Summary and conclusions

Approximately 70 000 symmetric three-jet events ($y_{\rm cut} = 0.1$ for the Durham algorithm) have been selected from 3×10^6 hadronic Z decays recorded by the ALEPH detector. From these events, 4 000 gluon jet candidates with a purity of 94.4% have been obtained by means of an impact parameter tagging method, which identifies jets containing heavy quarks. With these data properties of quark and gluon jets have been studied over a broad range of scales, covering hard and soft phenomena.

The jet broadening distribution and the differential one-subjet rate have been exploited to characterize the jet shape. These observables show a sensitivity to perturbative QCD at hard scales and are found to be compatible with the predictions of QCD-based Monte Carlo models.

Next, the internal structure of jets has been investigated using the subjet multiplicity distribution. By measuring the mean and the width of this distribution as a function of the subjet resolution scale, the transition from hard to soft QCD has been studied. In general, good agreement with the predictions of Monte Carlo generators was observed. It was found, however, that the subjet multiplicity distribution for quark jets predicted by HERWIG version 5.8 is significantly too broad at soft QCD scales, while the same quantity for gluon jets is in good agreement with the data. The mean subjet multiplicities were also compared with perturbative predictions, which show that leading and next-to-leading logarithmic terms are necessary in order to extend agreement down to softer QCD scales. For both quark and gluon jets, good agreement is achieved down to $y_0 \approx 10^{-3}$. For lower scales, the discrepancy between data and prediction is more pronounced for quark jets. The QCD colour factor C_A was determined from the mean subjet multiplicities and showed good agreement with the standard model value.

The properties of the subjet multiplicity distribution were also investigated as a function of jet energy. By comparing samples of jets with similar energies, the differences between quark and gluon jets were found to increase significantly.

Finally, a precise measurement of the fragmentation function for charged particles in quark and gluon jets has been carried out.

Acknowledgements

We would like to thank M.H. Seymour for many helpful discussions and for providing the motivation for many of the studies presented. We wish to thank our colleagues from the accelerator divisions for the successful operation of LEP. It is also a pleasure to thank the technical personnel of the collaborating institutions for their support in constructing and maintaining the ALEPH experiment. Those of the collaboration not from member states thank CERN for its hospitality.

References

[1] ALEPH Collaboration, Study of the subjet structure of quark and gluon jets, *Phys. Lett.* **B 346** (1995) 389.

[2] ALEPH Collaboration, Quark and Gluon Jet Properties in Symmetric Three-Jet Events, *Phys. Lett.* **B 384** (1996) 353.

[3] M.H. Seymour, *Phys. Lett.* **B 378** (1996) 279.

[4] ALEPH Collaboration, ALEPH: a detector for electron-positron annihilations at LEP, *Nucl. Instr. Meth.* **A 294** (1990) 121.

[5] W.J. Stirling, J. Phys. **G** *Nucl. Part. Phys.* **17** (1991) 1567.

[6] Frank Stephan, Untersuchung der Substruktur von Quarkjets und Gluonjets aus dem Z^0-Zerfall, Ph.D. thesis, University of Siegen, SI-97-21 (1997).

[7] Volker Büscher, Untersuchung der Struktur von Quark- und Gluonjets in Z-Zerfällen, diploma thesis, University of Siegen (1995).

[8] ALEPH Collaboration, Performance of the ALEPH detector at LEP, *Nucl. Instr. Meth.* **A 360** (1995) 481.

[9] T. Sjöstrand, *Comp. Phys. Comm.* **82** (1994) 74.

[10] J.E. Campagne and R. Zitoun, *Z. Phys.* **C 43** (1989) 469.

[11] ALEPH Collaboration, Properties of hadronic Z decays and test of QCD generators, *Z. Phys.* **C 55** (1992) 209.

[12] S. Catani, G. Turnock and B.R. Webber, *Phys. Lett.* **B295** (1992) 269.

[13] ALEPH Collaboration, A precise measurement of $\Gamma_Z \to b\bar{b}/\Gamma_Z \to$ hadrons, *Phys. Lett.* **B 313** (1993) 535.

[14] G. Marchesini et al., *Comp. Phys. Comm.* **67** (1992) 465.

[15] L. Lönnblad, *Comp. Phys. Comm.* **71** (1992) 15.

[16] ALEPH Collaboration, Studies of quantum chromodynamics with the ALEPH detector, CERN-PPE/96-186, to appear in *Physics Reports*.

[17] S. Catani and M.H. Seymour, private communication.

[18] ALEPH Collaboration, Measurements of the charged particle multiplicity distribution in restricted rapidity intervals, *Z. Phys.* **C 69** (1995) 15.

[19] M.H. Seymour, private communication.

[20] A. Bassetto, M. Ciafaloni, G. Marchesini, *Nucl. Phys.* **B 163** (1980) 477.

[21] E.D. Malaza and B.R. Webber, *Phys. Lett.* **B 149** (1984) 501.

[22] I.M. Dremin, *Physics-Uspekhi* **37**(8) (1994) 715.

[23] Yu.L. Dokshitzer, *Phys. Lett.* **B 305** (1993) 295.

[24] ALEPH Collaboration, A measurement of the QCD colour factors and a limit on the light gluino, *Z. Phys.* **C 76** (1997) 1.

[25] OPAL Collaboration, A measurement of the QCD colour factor ratios C_A/C_F and T_F/C_F from angular correlations in four-jet events, *Z. Phys.* **C 65** (1995) 367.

[26] DELPHI Collaboration, Measurement of the triple gluon vertex from double quark tagged 4-Jet events, *Phys. Lett.* **B414** (1997) 401.

[27] R.M. Barnett et al., *Physical Review* **D 54** (1996) 1.

[28] ALEPH Collaboration, The topology dependence of charged particle multiplicities in three-jet events, *Z. Phys.* **C 76** (1997) 191.

[29] OPAL Collaboration, A model independent measurement of quark and gluon jet properties and differences, *Z. Phys.* **C68** (1995) 179;
DELPHI Collaboration, Energy dependence of the differences between the quark and gluon jet fragmentation, *Z. Phys.* **C70** (1996) 179.

[30] V.N. Gribov und L.N. Lipatov, *Sov. J. Nucl. Phys.* **15** (1972) 78;
G. Altarelli und G. Parisi, *Nucl. Phys.* **B 126** (1977) 298;
Yu.L. Dokshitzer, *Sov. Phys. JETP* **46** (1977) 641.

[31] ALEPH Collaboration, Measurement of α_s from scaling violations in fragmentation functions in e^+e^- annihilation, *Phys. Lett.* **B 357** (1995) 487.

[32] P. Nason and B.R. Webber, *Nuclear Physics* **B 421** (1994) 473;
M. Dasgupta and B.R. Webber, *Nuclear Physics* **B 484** (1997) 247.

Interval of $B_{\rm jet}$	$\frac{1}{\sigma_{\rm q}}\frac{{\rm d}\sigma_{\rm q}}{{\rm d}B_{\rm jet}}$	$\frac{1}{\sigma_{\rm g}}\frac{{\rm d}\sigma_{\rm g}}{{\rm d}B_{\rm jet}}$
0.00 – 0.10	1.4204 ± 0.0220 ± 0.0864	0.2344 ± 0.0390 ± 0.0456
0.10 – 0.14	4.9261 ± 0.0623 ± 0.1374	1.1656 ± 0.1090 ± 0.1620
0.14 – 0.18	4.5405 ± 0.0740 ± 0.1840	2.2749 ± 0.1372 ± 0.2367
0.18 – 0.22	3.3971 ± 0.0793 ± 0.1326	2.9567 ± 0.1520 ± 0.1908
0.22 – 0.26	2.3027 ± 0.0804 ± 0.0900	3.2423 ± 0.1570 ± 0.1750
0.26 – 0.30	1.5427 ± 0.0787 ± 0.0977	3.2367 ± 0.1551 ± 0.2358
0.30 – 0.34	1.2420 ± 0.0687 ± 0.1095	2.5522 ± 0.1350 ± 0.2523
0.34 – 0.38	0.6978 ± 0.0697 ± 0.0696	2.5165 ± 0.1389 ± 0.1732
0.38 – 0.42	0.6320 ± 0.0631 ± 0.0713	1.9551 ± 0.1255 ± 0.1684
0.42 – 0.46	0.5464 ± 0.0549 ± 0.0745	1.4853 ± 0.1090 ± 0.1390
0.46 – 0.50	0.4404 ± 0.0452 ± 0.0489	1.0807 ± 0.0893 ± 0.1063
0.50 – 0.55	0.4036 ± 0.0332 ± 0.0822	0.6873 ± 0.0652 ± 0.1590
0.55 – 0.60	0.2987 ± 0.0270 ± 0.0500	0.4159 ± 0.0528 ± 0.1027
0.60 – 0.70	0.0724 ± 0.0160 ± 0.0244	0.2575 ± 0.0321 ± 0.0654
0.70 – 0.85	0.0077 ± 0.0015 ± 0.0041	0.0049 ± 0.0028 ± 0.0083

Table 1: The measured $B_{\rm jet}$ distribution for quark and gluon jets. The first error is statistical and the second is systematic.

Interval of L_2	$\frac{1}{\sigma_{\rm q}}\frac{{\rm d}\sigma_{\rm q}}{{\rm d}L_2}$	$\frac{1}{\sigma_{\rm g}}\frac{{\rm d}\sigma_{\rm g}}{{\rm d}L_2}$
2.50 – 3.00	0.0104 ± 0.0016 ± 0.0052	0.0116 ± 0.0033 ± 0.0118
3.00 – 3.50	0.0262 ± 0.0025 ± 0.0040	0.0330 ± 0.0049 ± 0.0086
3.50 – 4.00	0.0484 ± 0.0034 ± 0.0038	0.0653 ± 0.0067 ± 0.0047
4.00 – 4.50	0.0742 ± 0.0044 ± 0.0101	0.1203 ± 0.0086 ± 0.0201
4.50 – 5.00	0.0866 ± 0.0055 ± 0.0117	0.1950 ± 0.0109 ± 0.0220
5.00 – 5.50	0.1136 ± 0.0062 ± 0.0098	0.2556 ± 0.0123 ± 0.0183
5.50 – 6.00	0.1736 ± 0.0068 ± 0.0096	0.3011 ± 0.0134 ± 0.0105
6.00 – 6.50	0.2467 ± 0.0068 ± 0.0158	0.3005 ± 0.0131 ± 0.0323
6.50 – 7.00	0.2929 ± 0.0072 ± 0.0138	0.2923 ± 0.0140 ± 0.0235
7.00 – 7.50	0.3074 ± 0.0058 ± 0.0137	0.1814 ± 0.0109 ± 0.0263
7.50 – 8.00	0.2559 ± 0.0052 ± 0.0090	0.1282 ± 0.0098 ± 0.0174
8.00 – 8.50	0.1802 ± 0.0036 ± 0.0068	0.0544 ± 0.0065 ± 0.0099
8.50 – 9.00	0.1015 ± 0.0024 ± 0.0086	0.0240 ± 0.0040 ± 0.0069
9.00 – 9.50	0.0512 ± 0.0019 ± 0.0050	0.0105 ± 0.0033 ± 0.0045
9.50 – 10.00	0.0195 ± 0.0010 ± 0.0043	0.0025 ± 0.0017 ± 0.0041
10.00 – 10.50	0.0054 ± 0.0014 ± 0.0032	0.0058 ± 0.0028 ± 0.0073

Table 2: The measured distribution of $L_2 = -\ln y_2$ for quark and gluon jets. The first error is statistical and the second is systematic.

$\log_{10}(y_0)$	$\langle N_g - 1 \rangle(y_0)$	$\langle N_q - 1 \rangle(y_0)$	$R_N(y_0)$
-6.0	13.06 ± 0.09 ± 0.12	10.580 ± 0.048 ± 0.095	1.235 ± 0.014 ± 0.013
-5.8	11.90 ± 0.08 ± 0.17	9.578 ± 0.044 ± 0.079	1.242 ± 0.014 ± 0.013
-5.6	10.66 ± 0.07 ± 0.19	8.615 ± 0.039 ± 0.068	1.238 ± 0.014 ± 0.013
-5.4	9.55 ± 0.07 ± 0.17	7.739 ± 0.036 ± 0.059	1.234 ± 0.014 ± 0.013
-5.2	8.54 ± 0.06 ± 0.15	6.866 ± 0.032 ± 0.051	1.243 ± 0.014 ± 0.013
-5.0	7.54 ± 0.05 ± 0.11	6.030 ± 0.029 ± 0.044	1.250 ± 0.015 ± 0.014
-4.8	6.596 ± 0.049 ± 0.081	5.230 ± 0.026 ± 0.037	1.261 ± 0.015 ± 0.014
-4.6	5.716 ± 0.044 ± 0.059	4.469 ± 0.024 ± 0.032	1.279 ± 0.016 ± 0.015
-4.4	4.844 ± 0.039 ± 0.044	3.786 ± 0.021 ± 0.028	1.279 ± 0.017 ± 0.016
-4.2	4.101 ± 0.035 ± 0.034	3.132 ± 0.019 ± 0.024	1.309 ± 0.018 ± 0.017
-4.0	3.399 ± 0.031 ± 0.027	2.556 ± 0.016 ± 0.020	1.330 ± 0.020 ± 0.019
-3.8	2.793 ± 0.027 ± 0.023	2.037 ± 0.015 ± 0.018	1.371 ± 0.023 ± 0.021
-3.6	2.248 ± 0.024 ± 0.019	1.595 ± 0.013 ± 0.015	1.409 ± 0.026 ± 0.024
-3.4	1.777 ± 0.021 ± 0.017	1.217 ± 0.011 ± 0.013	1.461 ± 0.031 ± 0.027
-3.2	1.385 ± 0.019 ± 0.015	0.888 ± 0.010 ± 0.011	1.560 ± 0.039 ± 0.032
-3.0	1.052 ± 0.017 ± 0.014	0.6287 ± 0.0091 ± 0.0096	1.673 ± 0.050 ± 0.038
-2.8	0.767 ± 0.015 ± 0.013	0.4313 ± 0.0080 ± 0.0081	1.778 ± 0.067 ± 0.047
-2.6	0.539 ± 0.013 ± 0.012	0.2887 ± 0.0071 ± 0.0068	1.867 ± 0.091 ± 0.059
-2.4	0.364 ± 0.012 ± 0.011	0.1957 ± 0.0062 ± 0.0056	1.86 ± 0.12 ± 0.08
-2.2	0.242 ± 0.011 ± 0.009	0.1316 ± 0.0055 ± 0.0046	1.84 ± 0.16 ± 0.10
-2.0	0.1399 ± 0.0086 ± 0.0076	0.0884 ± 0.0044 ± 0.0037	1.58 ± 0.17 ± 0.15
-1.8	0.0718 ± 0.0065 ± 0.0058	0.0533 ± 0.0034 ± 0.0029	1.35 ± 0.20 ± 0.21
-1.6	0.0330 ± 0.0045 ± 0.0041	0.0262 ± 0.0024 ± 0.0022	1.26 ± 0.28 ± 0.32
-1.4	0.0171 ± 0.0043 ± 0.0028	0.0082 ± 0.0022 ± 0.0016	2.08 ± 1.05 ± 0.52
-1.2	0.0022 ± 0.0013 ± 0.0020	0.0034 ± 0.0007 ± 0.0011	0.66 ± 0.50 ± 0.86

Table 3: The mean subjet multiplicity for gluon jets, quark jets, and the ratio $R_N(y_0) = \langle N_g - 1 \rangle(y_0) \,/\, \langle N_q - 1 \rangle(y_0)$ for different values of the subjet resolution parameter y_0. The first error is statistical and the second is systematic. This table corresponds to the $E_{\rm jet}$-integrated case.

$\log_{10}(y_0)$	$\sigma_{\rm g}(y_0)$	$\sigma_{\rm q}(y_0)$	$R_\sigma(y_0)$
-6.0	4.021 ± 0.071 ± 0.099	3.823 ± 0.037 ± 0.046	1.052 ± 0.028 ± 0.037
-5.8	3.670 ± 0.065 ± 0.091	3.474 ± 0.034 ± 0.044	1.057 ± 0.029 ± 0.034
-5.6	3.272 ± 0.058 ± 0.084	3.145 ± 0.031 ± 0.043	1.040 ± 0.028 ± 0.034
-5.4	2.928 ± 0.051 ± 0.076	2.850 ± 0.027 ± 0.041	1.027 ± 0.027 ± 0.035
-5.2	2.649 ± 0.048 ± 0.069	2.559 ± 0.025 ± 0.038	1.035 ± 0.028 ± 0.035
-5.0	2.396 ± 0.044 ± 0.061	2.297 ± 0.023 ± 0.035	1.043 ± 0.029 ± 0.036
-4.8	2.138 ± 0.038 ± 0.054	2.065 ± 0.020 ± 0.030	1.035 ± 0.028 ± 0.036
-4.6	1.928 ± 0.035 ± 0.046	1.839 ± 0.018 ± 0.026	1.049 ± 0.029 ± 0.035
-4.4	1.709 ± 0.031 ± 0.039	1.647 ± 0.016 ± 0.022	1.038 ± 0.028 ± 0.034
-4.2	1.497 ± 0.027 ± 0.033	1.482 ± 0.014 ± 0.019	1.010 ± 0.027 ± 0.033
-4.0	1.334 ± 0.023 ± 0.027	1.324 ± 0.012 ± 0.016	1.007 ± 0.026 ± 0.031
-3.8	1.180 ± 0.021 ± 0.023	1.179 ± 0.011 ± 0.014	1.001 ± 0.027 ± 0.030
-3.6	1.072 ± 0.018 ± 0.019	1.037 ± 0.010 ± 0.012	1.034 ± 0.027 ± 0.029
-3.4	0.946 ± 0.017 ± 0.016	0.9279 ± 0.0087 ± 0.0099	1.019 ± 0.027 ± 0.028
-3.2	0.848 ± 0.014 ± 0.014	0.8156 ± 0.0075 ± 0.0085	1.039 ± 0.026 ± 0.027
-3.0	0.767 ± 0.013 ± 0.012	0.7071 ± 0.0068 ± 0.0074	1.084 ± 0.028 ± 0.027
-2.8	0.689 ± 0.011 ± 0.011	0.6004 ± 0.0057 ± 0.0064	1.147 ± 0.028 ± 0.027
-2.6	0.603 ± 0.009 ± 0.010	0.5002 ± 0.0048 ± 0.0056	1.205 ± 0.028 ± 0.029
-2.4	0.5220 ± 0.0083 ± 0.0096	0.4155 ± 0.0045 ± 0.0050	1.256 ± 0.033 ± 0.031
-2.2	0.4423 ± 0.0086 ± 0.0092	0.3469 ± 0.0046 ± 0.0046	1.275 ± 0.041 ± 0.036
-2.0	0.3505 ± 0.0098 ± 0.0090	0.2850 ± 0.0052 ± 0.0045	1.230 ± 0.056 ± 0.045
-1.8	0.260 ± 0.011 ± 0.009	0.2232 ± 0.0059 ± 0.0046	1.164 ± 0.079 ± 0.063
-1.6	0.179 ± 0.012 ± 0.010	0.1593 ± 0.0063 ± 0.0053	1.12 ± 0.12 ± 0.10
-1.4	0.130 ± 0.016 ± 0.012	0.0927 ± 0.0083 ± 0.0068	1.40 ± 0.30 ± 0.20
-1.2	0.047 ± 0.013 ± 0.018	0.059 ± 0.007 ± 0.010	0.81 ± 0.32 ± 0.50

Table 4: The standard deviation of the subjet multiplicity distribution for gluon jets, quark jets, and the ratio $R_\sigma(y_0) = \sigma_{\rm g}(y_0)$ / $\sigma_{\rm q}(y_0)$ for different values of the subjet resolution parameter y_0. The first error is statistical and the second is systematic. This table corresponds to the $E_{\rm jet}$-integrated case.

Interval of x_E	$\frac{1}{\sigma_{\rm q}}\frac{{\rm d}\sigma_{\rm q}}{{\rm d}x_E}$	$\frac{1}{\sigma_{\rm g}}\frac{{\rm d}\sigma_{\rm g}}{{\rm d}x_E}$
0.00 – 0.05	97.885 ± 0.521 ± 1.160	131.016 ± 1.022 ± 2.519
0.05 – 0.10	35.595 ± 0.283 ± 0.578	46.715 ± 0.551 ± 0.962
0.10 – 0.15	15.345 ± 0.177 ± 0.268	18.821 ± 0.343 ± 0.403
0.15 – 0.25	6.528 ± 0.074 ± 0.115	6.434 ± 0.142 ± 0.175
0.25 – 0.35	2.394 ± 0.039 ± 0.053	1.706 ± 0.074 ± 0.066
0.35 – 0.55	0.712 ± 0.013 ± 0.019	0.381 ± 0.024 ± 0.035
0.55 – 0.80	0.109 ± 0.004 ± 0.007	0.043 ± 0.008 ± 0.016

Table 5: The measured fragmentation function for quark and gluon jets. The first error is statistical and the second is systematic.